CEBAF Program Advisory Committee Eight Cover Sheet

This proposal must be received by close of business on Thursday, April 14, 1994 at:

CEBAF
User Liaison Office, Mail Stop 12 B
12000 Jefferson Avenue
Newport News, VA 23606

Proposal Title

STUDY OF THE AXIAL ANOMALY USING THE $\gamma\pi^+ \rightarrow \pi^+\pi^0$ REATION NEAR THRESHOLD.

Contact Person

Name: R. A. MISKIMEN
Institution: UNIVERSITY OF MASSACHUSETTS
Address: DEPARTMENT OF PHYSICS AND ASTRONOMY
Address: UNIVERSITY OF MASSACHUSETTS
City, State ZIP/Country: AMHERST, MA 01003
Phone: (413) 545-2480 **FAX:** (413) 545-4884
E-Mail → Internet: MISKIMEN@phast.UMass.edu

Experimental Hall: B
Total Days Requested for Approval: 58
Minimum and Maximum Beam Energies (GeV): E_γ =0.5 - 2.25 GeV
Minimum and Maximum Beam Currents (μAmps): 10^7 photons/sec.

CEBAF Use Only

Receipt Date: 4/14/93 PR 94-019

By:

Study of the Axial Anomaly using the $\gamma\pi^+ \rightarrow \pi^+\pi^0$ Reaction Near Threshold

B. Mecking, E. S. Smith, and A.Yegneswaran
CEBAF, Newport News, Virginia

P. Degtyarenko, L. Elouadrhiri, R. S. Hicks, R. A. Miskimen,
G. A. Peterson, and K. Wang
University of Massachusetts, Amherst, MA

A. M. Bernstein
Massachusetts Institute of Technology, Cambridge, MA

J. Calarco, and M. Kennedy
University of New Hampshire, Durham, NH

J. Napolitano
Rensselaer Polytechnic Institute, Troy, NY

and the CLAS

REAL PHOTON WORKING GROUP

Spokespersons: R. A. Miskimen, K. Wang, and A. Yegneswaran

Abstract

We propose to measure $\gamma\pi^+ \to \pi^+\pi^0$ near threshold. The $\gamma\pi^+ \to \pi^+\pi^0$ reaction will be studied by measuring $\gamma p \to \pi^+\pi^0 n$ cross sections near $t \approx -m_\pi^2$ using tagged photons with energies between 1 and 2 GeV, and the CLAS detector. The $\gamma \to 3\pi$ structure function, $F^{3\pi}$, is related to the $\pi^0 \to \gamma\gamma$ amplitude by PCAC and is predicted by the Wess-Zumino-Witten effective Lagrangian in the limit of zero momentum. $F^{3\pi}$ will be measured in the physical region and compared with models for the momentum dependence of the structure function.

1 Introduction

The QCD Lagrangian is difficult to solve at medium and low energies due to the large size of the strong interaction coupling constant. It is for this reason that there has been considerable theoretical effort to develop, as suggested by Weinberg[1], effective Lagrangians based on the symmetries of QCD. In the limit of massless quarks, QCD exhibits chiral symmetry. The left-handed and right-handed components of the quark spinor field decouple, and QCD has an exact $SU(3)_L \times SU(3)_R$ symmetry. This symmetry is dynamically broken resulting in eight massless Goldstone bosons, which are identified with π, K, and η.

By expanding an effective chiral Lagrangian in powers of field derivatives, chiral perturbation theory (χPT) can predict low energy scattering reactions and decays[2]. The energy scale of the expansion is of order $4\pi F_\pi \approx 1GeV$, where F_π is the pion decay constant, $F_\pi = 93.1 \pm 0.1$ MeV. The effective Lagrangians have phenomenological constants which must be constrained from known reactions. For the most general order four Lagrangian (four powers of field derivatives) there are ten arbitrary constants[3].

Calculations based on chiral symmetry and experimental tests of these QCD based predictions are among the most important low energy tests of the standard model in progress. Recently there has been considerable theoretical and experimental activity in the areas of threshold π^0 photoproduction, $\pi\pi$ scattering, and hadron polarizabilities[4]. In this proposal we request approval for a study of the axial anomaly using the $\gamma\pi^+ \to \pi^+\pi^0$ reaction near threshold. Cross sections for $\gamma\pi^+ \to \pi^+\pi^0$ will be obtained from measurements of $\gamma p \to \pi^+\pi^0 n$ near $t \approx -m_\pi^2$. Figure 1 shows the t-channel pion

exchange diagram for the reaction and how it is related to the $\gamma\pi^+ \rightarrow \pi^+\pi^0$ vertex.

2 The axial anomaly and $\gamma \rightarrow 3\pi$

Symmetry breaking in physics can occur through several different mechanisms. These mechanisms include explicit, spontaneous, dynamical, and quantum mechanical symmetry breaking terms. Quantum mechanical symmetry breaking occurs when a symmetry that is present in a classical Lagrangian is broken when the theory is quantized. This condition leads to the occurance of an "anomaly". In early theoretical investigations of π^0 decay through the partially conserved axial current (PCAC) and current algebra, it was discovered that an anomalous axial current is needed to explain the π^0 decay rate[5]. Later, with the development of effective chiral Lagrangians, it was clear that the symmetry properties of these Lagrangians forbid the transition between an even and odd number of mesons, although these transitions are allowed by QCD and are observed in reactions such as $\pi^0 \rightarrow \gamma\gamma$ and $K\overline{K} \rightarrow \pi^+\pi^-\pi^0$. To amend this problem the Wess-Zumino-Witten effective Lagrangian was constructed[6, 7]. While we do not reproduce here the structure of the axial anomaly in the Lagrangian, it is important to note that the expression has a known coefficient that depends only on F_π, and on the number of colors, N_c (in chiral theories F_π is a fundamental constant, appearing in calculations with every field deriviative). In this respect the axial anomaly is unlike other terms in the effective Lagrangian which have free parameters that must be adjusted to agree with experiment.

The axial anomaly allows the $\pi^0 \rightarrow \gamma\gamma$ reaction to proceed at a significant rate, providing one of the widely noted methods for measuring the number of colors. The predicted amplitude for $\pi^0 \rightarrow 2\gamma$ is

$$A^{th}_{\pi\gamma\gamma} = \frac{\alpha N_c}{3\pi F_\pi} = 0.025\ GeV^{-1}$$

for $N_c = 3$. The experimental amplitude, $A^{exp}_{\pi\gamma\gamma} = (0.0240 \pm 0.0003) GeV^{-1}$[4], is in good agreement with the predicted amplitude. This is generally regarded as an important triumph of QCD, both as a test of $N_c = 3$ and of the symmetries and anomalies of the theory.

The axial anomaly also predicts amplitudes for the reactions

$$\gamma \rightarrow \pi^+\pi^-\pi^0$$

$$\gamma \rightarrow K^+K^-\pi^0$$

$$\gamma \rightarrow \pi^+\pi^-\eta_8$$

The $\gamma \rightarrow 3\pi$ amplitude, $F^{3\pi}$, was first derived from the $\pi^0 \rightarrow \gamma\gamma$ amplitude using PCAC[8, 9, 10], and later from the Wess-Zumino-Witten effective chiral Lagrangian. The amplitude, given by

$$F^{3\pi} = \frac{eN_c}{12\pi^2 F_\pi^3} = 9.5 GeV^{-3}$$

is similar to the π^0 decay amplitude in that it depends only on N_c and the pion decay constant.

The amplitude predicted from the axial anomaly does not agree with the results of vector meson dominance (VMD). Working in the low energy limit of a $\gamma \rightarrow \pi\rho \rightarrow 3\pi$ model Cohen[11] has shown that the $\gamma \rightarrow 3\pi$ amplitude is given by

$$F^{3\pi}_{VMD} = \frac{3}{2} F^{3\pi}$$

To enforce consistency with PCAC, Cohen indicates that "short range" contributions to the amplitude, not included in the VMD model, are needed to reproduce the PCAC result.

Using the $\gamma p \rightarrow \pi^+\pi^0 n$ kinematics of Figure 1 we define $s = (k_1 + k_2)^2$, $t' = (q - k_1)^2$, and $u = (q - k_2)^2$. The vectors q, k_1, k_2, and k_3 are the four-vectors of the photon, outgoing π^+ and π^0, and virtual pion, respectively. The constant chiral value for $F^{3\pi}$ is strictly valid in the limit where all pairs of invariant masses are zero, $q^2 = s = t' = u = 0$. In the physical region, where $s > 4m_\pi^2$ and $t = k_3^2 < 0$, $F^{3\pi}$ acquires momentum dependence on q^2, s, t', and u. It is generally expected that VMD can yield the momentum dependence of $F^{3\pi}$. Figure 2 shows the s dependence of $F^{3\pi}$ for several different theoretical models, which are described in detail in Appendix A.

There is only one experimental determination of $F^{3\pi}$ that needs consideration here. This measurement is the 40 GeV/c $\pi^- A \rightarrow \pi^-\pi^0 A$ radiative production experiment performed by Antipov *et al.* at Serpukhov[12].

To enhance pion pair production in the Coulomb field over hadronic backgrounds, the data for this experiment were taken at low momentum transfer, $q^2 < 2 \times 10^{-3}\ GeV^2/c^2$. The targets were C, Al and Fe. Figure 2 shows the value obtained for $F^{3\pi}$ averaged over the range $s = 5 - 11m_\pi^2$ and compared to various models for $F^{3\pi}(s)$. The result obtained from this measurement, $F^{exp} = 12.9 \pm 0.9 \pm 0.5 GeV^{-3}$, is higher than the chiral result $F^{theo} = 9.5 GeV^{-3}$. Taken literally it would imply the number of colors is four. The data point is also in agreement with the $\gamma \rightarrow \pi\rho$ model.

Hadronic backgrounds are a problem with the radiative production experiment. Because the $\gamma \rightarrow 3\pi$ reaction has an electromagnetic nature and the $\pi A \rightarrow 2\pi A$ reaction can be hadronic, the signal-to-background ratio will be reduced by the ratio of electromagnetic to strong interactions. The experiment also suffered from poor statistics; their final sample contains approximately 200 events.

We conclude that a high statistics measurement of $F^{3\pi}$ using real photons is needed. While the radiative production experiments were statistics limited, with real photons it will be possible to acquire high statistics (several thousand events) in relatively short running periods (several weeks). Compared to radiative production with pion beams, the advantage to a photon induced reaction near the pion pole is that both signal and backgrounds will be electromagnetic in origin, which should be optimal for background rejection. In addition, the use of real photons will eliminate ω-pole contributions to the amplitude (see Appendix A).

3 Overview of the experiment

We propose to measure $F^{3\pi}$ in the $\gamma\pi^+ \rightarrow \pi^+\pi^0$ reaction near threshold, $s < 15m_\pi^2$. The $\gamma\pi^+ \rightarrow \pi^+\pi^0$ reaction will be studied by measuring $\gamma p \rightarrow \pi^+\pi^0 n$ cross sections near $t \approx -m_\pi^2$. We plan to use tagged photons with energies between 1 and 2 GeV. The π^+ will be detected using the CLAS drift chambers and time-of-flight system, and the π^0 using the electromagnetic calorimeters. Because we do not require the detection of the recoil nucleon, it will be possible to take data at the lowest values of $|t|$ which are kinematically allowed. For $s = 10\ m_\pi^2$, the minimum values of $|t|$ are 0.61 m_π^2 and 0.13 m_π^2 for $E_\gamma = 1.0$ and 2.0 GeV, respectively. The experiment will be able to extract $F^{3\pi}$ at several values of s over the interval $6 < s < 15\ m_\pi^2$ so that

any dependence of $F^{3\pi}$ on s can be determined and compared to theoretical models.

Backgrounds from other reactions that produce $\pi^+\pi^0$ final states are a concern for this experiment (see Appendix B for a detailed discussion). We request a broad photon tagging interval, from approximately 1 to 2 GeV in photon energy, to help us understand the characteristics of the backgrounds and to optimize signal-to-background. The dominant physics backgrounds will be from $\gamma p \to \Delta\pi$ and $\gamma p \to N^* \to \rho^+ n$ reactions. These backgrounds can be minimized by placing cuts on s, t, the π^+ center-of-mass angle θ_π, and the πn invariant mass.

3.1 Cross sections for $\gamma p \to \pi^+\pi^0 n$

The cross section for the reaction $\gamma\pi \to \pi\pi$ is given by[13, 14]

$$\frac{d\sigma_{\gamma\pi\to\pi\pi}}{d\tau} = \frac{(F^{3\pi})^2}{128\pi}\frac{1}{4}(s-4m_\pi^2)sin^2\theta_\pi$$

where in the kinematics of Figure 1 $\tau = (k_3 - k_1)^2$, $s = (k_1 + k_2)^2$, and θ_π is the π^+ scattering angle relative to the photon direction in the center of mass frame. It is generally more convenient to work with cross sections differential in $d\Omega$. By using the kinematic relationship

$$\tau = \frac{1}{2}\left[2t + m_\pi^2 - s - (s-m_\pi^2)\sqrt{1-\frac{4m_\pi^2}{s}}cos\theta_\pi\right]$$

where $t = k_3^2$, the differential and total cross sections are derived to be

$$\frac{d\sigma_{\gamma\pi\to\pi\pi}}{d\Omega} = \frac{(F^{3\pi})^2}{128\pi}\frac{s}{16\pi}\left(1-\frac{4m_\pi^2}{s}\right)^{3/2}(s-m_\pi^2)sin^2\theta_\pi$$

$$\sigma_{\gamma\pi\to\pi\pi} = \frac{(F^{3\pi})^2}{128\pi}\frac{s}{6}\left(1-\frac{4m_\pi^2}{s}\right)^{3/2}(s-m_\pi^2)$$

For incident real photons, Aibergenov *et al.*[15] have obtained the general form of $\gamma\pi^+$ cross sections near the pion pole as:

$$\frac{d^2\sigma}{dtds} = \left(\frac{g^2}{4\pi}\right)\left(\frac{s-m_\pi^2}{8\pi m_N^2 E_\gamma^2}\right)\left(\frac{-t}{(t-m_\pi^2)^2}\right)F_{N\pi N}^2(t)\sigma_{\gamma\pi\to\pi\pi} \qquad (1)$$

where $g^2/4\pi = 14.7$ is the π-nucleon coupling constant. The form factor $F_{N\pi N}(t)$ describes the momentum dependence of the πN coupling. To a good approximation this can be represented by the axial form factor of the nucleon normalized to one at $t = 0$

$$F_{N\pi N}(t) = \frac{1}{\left(1 - \frac{t}{M_A^2}\right)^2}$$

and M_A is the axial mass parameter $M_A \approx 0.95$ GeV.

Figure 3 shows differential cross sections $d^2\sigma/dtds$ as a function of s for $E_\gamma = 1.5$ GeV and $t = -m_\pi^2$. $F^{3\pi}$ was assumed to have a constant value of 9.5 GeV^{-3}. The cross sections increase with s approximately as s^3. Cross sections at other values of E_γ, t, or $F^{3\pi}$ can be obtained by scaling the plotted cross sections by the appropriate kinematic factors, given in Equation 1. Figure 4 is a plot of the differential cross section $d^2\sigma/dtds$ as a function of t for $E_\gamma = 1.5$ GeV and $s = 10m_\pi^2$. The figure shows that for decreasing $|t|$ the cross sections are increasing approximately as $1/|t|$ with the maximum cross section at $t = -m_\pi^2$.

3.2 Event simulation: acceptance

To model $\gamma p \rightarrow \pi^+\pi^0 n$ events we have used the CLAS event simulation program "SDA" augmented with the electromagnetic calorimeter response. The calorimeter was assumed to be 100% efficient for photon events that fell within the fiducial volume of the detector. For compatibility with previously approved experiments[16], all of our simulations assume a magnetic field set to 20% of full field B_0, such that positive particles are bent outward.

For this measurement we require the detection of the π^+ and both photons from the π^0 decay. Figure 5 is a typical one-event-display from SDA for an accepted $\pi^+\pi^0$ event at $E_\gamma = 1.5$ GeV. Because of the $sin^2\theta_\pi$ distribution of the pions in the $\pi^+\pi^0$ center-of-mass frame, the acceptance of these events in the CLAS detector is good. Figure 6 shows the π^+ angular distribution for accepted events in the $\pi^+\pi^0$ center-of-mass frame at $s = 10\ m_\pi^2$ and for t distributed by $-t/(t-1)^2 F_{N\pi N}^2(t)$ over the interval $0 < |t| < 10m_\pi^2$. The solid curve in the figure is $sin^2\theta_\pi$ scaled to the Monte Carlo data. Comparison of the data with the curve indicates that acceptance is good over much of the angular range for the $\pi^+\pi^0$. The π^+ momentum distribution for the

accepted events is shown in figure 7. With a momentum distribution peaking at approximately 0.75 GeV/c, there will be no problem in using time-of-flight to distinguish between π^+, K^+ and protons[17].

For $E_\gamma = 1.5$ GeV, the calculated acceptance as a function of s and t is shown in Table 1. The acceptance calculation was based on 1000 input events per kinematic point. Because of the 3-body final state, the quantities s and t do not completely define the kinematics. The selection of the π^+ angle relative to the photon direction in the $\pi\pi$ C.M. frame was weighted by the $sin^2\theta_\pi$ factor of the angular distribution. Table 1 shows that acceptances vary from 10 to 20% for variations in s from 6 to 14 m_π^2, and variations in t from -1 to -9 m_π^2. The table also shows that for $s \approx 10$ the variation of acceptance with t is relatively slow.

Table 2 shows the calculated acceptance as a function of E_γ and s for $t = -2m_\pi^2$. Acceptance calculation was based on 1000 input events per kinematic point. In terms of acceptance and cross sections, which vary as $\sigma \approx s^3/E_\gamma^2$, high photon energies ($\approx$ 2 GeV) will be most suited for taking data near $s \approx 14m_\pi^2$. Low photon energies ($\approx$ 1 GeV) afford the possibility of taking data over a range in s from 6 to 14 m_π^2.

3.3 Event simulation: resolution

For event simulation the energy resolution of the electromagnetic calorimeter was taken as $8.5\%/\sqrt{E}$[17]. The $\gamma\gamma$ invariant mass distribution from π^0 decay at $E_\gamma = 1.5$ GeV, $s = 10m_\pi^2$ and t distributed as given by Equation 1 is shown in Figure 8. The calculated π^0 mass resolution is 40 MeV FWHM.

The resolution in $t = (q - k_1 - k_2)^2$ and to a lesser extent the resolutions in $s = (k_1 + k_2)^2$, $t' = (q - k_2)^2$, and $u = (q - k_1)^2$ are limited by the calorimeter energy resolution. To enhance the resolution, we plan to utilize the kinematic constraints offered by the $\pi^0 \rightarrow \gamma\gamma$ reaction. The $\gamma\gamma$ invariant mass squared is given by

$$m_{\gamma\gamma}^2 = 2E_1E_2\,(1 - cos\theta)$$

where θ is the opening angle, and E_1 and E_2 are the energies of the two photons, all in the laboratory system. If it is assumed that the two photons result from π^0 decay and that the resolution in θ is good compared to the resolution in E_1 and E_2, then the product of photon energies is determined

by the opening angle and is given by

$$E_1 E_2 = \frac{m_\pi^2}{2(1 - cos\theta)}$$

With a spatial resolution in the calorimeters on the order of 2-3 cm at a distance 4 meters from the target, the $m_{\gamma\gamma}^2$ resolution is dominated by the energy resolution in E_1 and E_2 and the above equation is a good measure of $E_1 E_2$. If t, s, t' and u were functions solely of the energy product defined by $P \equiv E_1 E_2$, then it would be possible to make exact corrections to these quantities. However, they are functions of E_1 and P, and it is necessary to select the "best" pair of energies, E_1' and E_2', consistent with $P = E_1' E_2'$. To make resolution corrections we propose to minimize χ^2 with respect to E_1',

$$\chi^2(E_1') = \frac{(E_1' - E_1)^2}{\sigma_{E_1}^2} + \frac{(P/E_1' - E_2)^2}{\sigma_{E_2}^2}$$

where E_1, E_2, σ_{E_1}, and σ_{E_2} are the measured photon energies and resolutions.

For calculations of t it most advantagous to use the expression $t = s + t' + u - 2m_\pi^2$ since it involves squares of four-vectors with cross terms in $E_1 E_2$ that are well constrained. Figure 9 shows the resolution functions for t, s, t', and u after corrections. For $s = 10m_\pi^2$, and $E_\gamma = 1.5$ GeV, the resolutions in sigma for t, s, t', and u are 0.32, 0.43, 0.38, and 0.06 m_π^2, respectively.

To summarize our discussion of acceptance and resolution, we plot in Figure 10 the t distribution for accepted events for $s = 10\ m_\pi^2$, and $E_\gamma = 1.5$ GeV. The t distribution from Equation 1 was used as input. The effects of acceptance and resolution are included in the Monte Carlo and are reflected in the data. The data clearly show peaking at $t \approx -m_\pi^2$, with a drop to zero as $t \to 0$. The solid curve in the figure shows the t dependence of Equation 1 scaled to fit the data at $t = -2m_\pi^2$. The correspondence with Monte Carlo data is good except for $|t| < 2m_\pi^2$ where it is necessary to include the effects of resolution and decreasing acceptance.

3.4 Data analysis

A completely model-independent analysis of the data uses the Chew-Low extrapolation technique[18]. One of the variations of this method is to form the product of the cross section and $(t - m_\pi^2)^2$, denoted by $f(t)$, and then

extrapolate $f(t)$ to the pion pole, $t \rightarrow m_\pi^2$. Generally this is done by fitting the data to a polynomial,

$$(t-m_\pi^2)^2\frac{d^2\sigma}{dtds} \equiv f(t) = c_0 + c_1(t-m_\pi^2) + c_2(t-m_\pi^2)^2 + c_3(t-m_\pi^2)^3 + ...$$

By going to $O(t-m_\pi^2)^3$ it is generally possible to make the extrapolation model independent. Furthermore, the extrapolation to the pion-pole is independent of the presence of backgrounds or interference terms, which at lowest order are present in the $O(t-m_\pi^2)$ term. Using Equation 1, the cross section at the pion-pole is given by

$$f(m_\pi^2) = c_0 = \left(\frac{-g^2}{4\pi}\right)\left(\frac{s-m_\pi^2}{8\pi m_N^2 E_\gamma^2}\right) m_\pi^2 \sigma_{\gamma\pi\rightarrow\pi\pi}$$

While the Chew-Low method is model independent, the background and interference terms limit the accuracy of the extrapolation. These terms may cause $f(0) > 0$ and, contrary to claims in the literature[15], it is not realistic to constrain the polynomial fit by $f(0) = 0$. The background terms also induce quadratic curvature in $f(t)$, which makes extrapolations to the pion-pole difficult. For this reason we propose to use the Chew-Low method only in kinematic regions where the background terms are small, primarily at high photon energies and high s values. For regions of high background contamination we propose to utilize a model-dependent extrapolation, and fit the data to functions such as

$$(t-m_\pi^2)^2\frac{d^2\sigma}{dtds} \equiv f(t) = c_0[1+\alpha(t-m_\pi^2)]tF_{N\pi N}^2(t) + c_1[1+\beta t](t-m_\pi^2)^2$$

where c_0 has the same relation to $\sigma_{\gamma\pi\rightarrow\pi\pi}$ as previously discussed. This function assumes a linear t dependence for $\sigma_{\gamma\pi\rightarrow\pi\pi}$ near the pole, an assumption supported by the calculations presented in Figure 2. In principle, α could be fitted to the data, although greater accuracy in c_0 can be obtained by fixing α from model calculations. The fitted function also assumes a linear background and no interference terms (ie. no terms in $(t-m_\pi^2)$). The precise form used for the parameterization of the background is not important if the shape can be fixed by the data. For example, it should be possible to obtain a good measure of the t distribution of the backgrounds events by going either to small s (the true cross section goes as $\approx s^3$), or to s values near the ρ.

Data from $\gamma n \rightarrow \rho^- p$ indicates that $\beta \approx 0.03 m_\pi^{-2}$ for the ρ^+ background (see Appendix B).

Figure 11 shows simulated data assuming a pessimistic signal-to-background ratio of 1:2 for $t = -m_\pi^2$, and $\alpha = 0$ and $\beta = 0.03 m_\pi^{-2}$. To simplify our analysis we have not included the effects of acceptance or resolution in the data, since we do not believe these will be limiting factors. In the distribution we assumed 100 true events/m_π^2 at $t = -m_\pi^2$. Given a 58 day run on proton at an incident energy of 2.4 GeV and a tagging rate of 10^7 photons per second, this will be achievable at $s = 10\ m_\pi^2$ and a bin width of $\Delta s = m_\pi^2$. The curves in the figure show the results of the model-dependent fit assuming fixed $\alpha = 0$ and $\beta = 0.03 m_\pi^{-2}$. The solid curve shows the fit to the signal background, and the dashed curve indicates the fitted background. The error in $\sigma_{\gamma\pi \rightarrow \pi\pi}$ resulting from the fit is $\pm 16\%$, which gives an amplitude error in $F^{3\pi}$ of $\pm 8\%$. We conclude that even with significant backgrounds it is feasible to measure $F^{3\pi}$ at the 10% level for values of s as small as $\approx 10\ m_\pi^{-2}$.

4 Run conditions and expected results

The data acquisition trigger should be one charged track in the CLAS and a tagged electron in the Tagger. Positive particles should be bent outward in the CLAS, and the magnetic field should be set to the highest value that is compatable with other experiments. For our purposes a magnetic field set to 20% of full field is adequate, and it maintains compatability with other approved experiments[16].

The electron beam energy should be 2.4 GeV, and the photon tagging interval should be over the full tagging interval from 0.2 to 0.95 of E_0. The wide range in photon energies, from 500 MeV to 2.3 GeV, will allow us to optimize our signal-to-background. Because the tagged photon flux varies as $1/E_\gamma$, the low energy photons should be pre-scaled. The prescaling plan worked out by the spokespersons of experiments E89-004, E89-024, E91-008, and E93-033 is acceptable to us. This plan calls for prescale factors of 1/16 for photon energies up to 0.85 GeV, 1/4 up to 1.4 GeV, and full rate beyond 1.4 GeV[19].

Our beam request is based upon obtaining 100 true events/m_π^4 at $t = -m_\pi^2$ and $s = 10 m_\pi^2$. For average cross sections and acceptances we have used the values at $E_\gamma = 1.5$ GeV, and we assumed an inefficiency from data cuts

of 50% (see Appendix B for details). Taking a tagger rate of 10^7 photons per second, and a liquid hydrogen target 10 cm long, we require 58 days of running at 2.4 GeV with detector conditions as stated above.

Figure 2 shows the anticipated errors in $F^{3\pi}$ for the proposed measurement as a function of s. In calculating the errors, a 10% systematic error in the cross section was added in quadrature, and it was assumed that the errors are not background limited. Under these conditions measurements down to $s \approx 7m_\pi^2$ are possible. The data are primarily systematics limited, not statistics limited, at values of s as small as 9 m_π^2. Compared to the data point of Antipov *et al.*, the proposed experiment will measure $F^{3\pi}$ with greater accuracy, and the data can be compared with models for the momentum dependence of $F^{3\pi}$.

5 Future extension using linearly polarized photons

The use of linearly polarized tagged photons provides a powerful means of identifying the t-channel pion exchange mechanism of Figure 1. In the $\pi^+\pi^0$ rest frame the angular distribution for pseudo-scalar (ie. pion) exchange is

$$W(cos\theta, \phi) = \frac{3}{8\pi} sin^2\theta(1 - \epsilon\ cos2\phi)$$

where ϵ is the photon polarization, and θ and ϕ are the polar and azimuthal angles of the pion relative to the photon direction and polarization. Therefore, for pseudo-scalar exchange, the pions are preferentially emitted at 90° to the direction of the photon electric vector. In general, this will not be the case for $\gamma p \rightarrow \pi\Delta$ and $\gamma p \rightarrow \rho^+ n$ reaction mechanisms.

At present there are two proposals under consideration for providing linearly polarized tagged photons in Hall B. One method is to produce coherent bremsstrahlung from a diamond crystal[26]. The technique produces approximately 40% polarization at $E_\gamma \approx 2$ GeV for an incident electron energy of 4 GeV. At 2 GeV the polarization could be determined by measuring a purely diffractive process, such as ρ^0 photo-production at low t, where the azimuthal distribution goes as $1 + \epsilon\ cos2\phi$. The other polarization technique uses laser backscattering from the electron beam[27]. In this case the linearly polarized laser light is contained within an optical cavity and a high current electron

beam passes through the cavity. High polarization, nearly 100%, can be obtained with this technique.

We plan to follow the development of these two linearly polarized photon sources. At some future date we will consider an extension of this proposal to study the axial anomaly using the $\vec{\gamma}\pi^+ \rightarrow \pi^+\pi^0$ reaction near threshold.

6 Summary

We request approval for a measurement of the $\gamma\pi^+ \rightarrow \pi^+\pi^0$ reaction near threshold. This reaction can be studied by measuring $\gamma p \rightarrow \pi^+\pi^0 n$ cross sections near $t \approx -m_\pi^2$. The $\gamma \rightarrow 3\pi$ structure function obtained from the data, $F^{3\pi}$, is related to $\pi^0 \rightarrow \gamma\gamma$ by PCAC and is predicted by the Wess-Zumino-Witten effective chiral Lagrangian without free parameters. To perform this measurement we request the following running conditions:

- Electron beam energy =2.4 GeV
- Liquid proton target
- Full tagging interval from 20% to 95% of full energy
- Tagging rate of 10^7 photons/s
- 58 days of CLAS operation
- Magnetic field set to bend positive particles outward
- Magnetic field not to be less than 20% of full field
- Prescaling of low energy tagged photons

A Momentum dependence of $F^{3\pi}$

The chiral amplitude is strictly valid in the limit $q^2 = s = t' = u = 0$. By using incident real photons $q^2 = 0$. However, in the physical region, where $s > 4m_\pi^2$ and $t < 0$, the quantities s, t', and u are non-zero. For the proposed measurement (incident real photon on a virtual pion, and two real outgoing pions) the relation between s, t', u, and t is

$$t = s + t' + u - 2m_\pi^2$$

Evaluating this expression for $s = 10m_\pi^2$ and small $|t|$ gives $t' \approx u \approx -5m_\pi^2$.

In the physical region it is expected that vector meson dominance (VMD) can yield the momentum dependence of $F^{3\pi}$. There have been several theoretical approaches to this problem. Terent'ev[20] considered the vector-meson pole diagrams shown in Figure 12 as corrections to $F^{3\pi}(0)$. The momentum dependence of $F^{3\pi}$ is given by

$$F^{3\pi}(s,t',u,q^2) = F^{3\pi}(0)\left[1 + C_\rho e^{i\delta}\left(\frac{s}{m_\rho^2 - s} + \frac{t'}{m_\rho^2 - t'} + \frac{u}{m_\rho^2 - u}\right) + C_\omega e^{i\delta'}\frac{q^2}{m_\omega^2 - q^2}\right]$$

$$C_\rho = \frac{2g_{\rho\pi\pi}g_{\rho\pi\gamma}}{m_\rho^3 F^{3\pi}(0)}$$

where $g_{\rho\pi\pi}$ and $g_{\rho\pi\gamma}$ are the coupling constants determined via the partial widths of the ρ meson,

$$\Gamma(\rho \to \pi\pi) = \frac{g_{\rho\pi\pi}^2 m_\rho}{48\pi}\left[1 - 4\frac{m_\pi^2}{m_\rho^2}\right]^{3/2}$$

$$\Gamma(\rho \to \pi\gamma) = \frac{g_{\rho\pi\gamma}^2 m_\rho}{96\pi}\left[1 - \frac{m_\pi^2}{m_\rho^2}\right]^3$$

and δ and δ' are unknown relative phases. Evaluating the above equations gives $C_\rho \approx 0.434$. There are similar expressions[12] for C_ω, and these give $C_\omega \approx 3$. An important advantage for a real photon measurement ($q^2 = 0$) is that the ω-pole contribution vanishes.

In an alternate approach Rudaz [21] considered VMD and the axial anomaly term to provide equivalent descriptions of the $\gamma \to 3\pi$ vertex, requiring consistency between the VMD and PCAC methods. The momentum dependence

of $F^{3\pi}$ in this prescription is given by

$$F^{3\pi}(s,t',u) = F^{3\pi}(0)\frac{m_\omega^2}{m_\omega^2 - q^2}\frac{1}{3}m_\rho^2\left(\frac{1}{m_\rho^2 - s} + \frac{1}{m_\rho^2 - t'} + \frac{1}{m_\rho^2 - u}\right)$$

In this model $F^{3\pi}(s,t',u)$ normalizes to $F^{3\pi}(0)$ at zero energy, with no unknown phases.

Most recently Bijnens *et al.*[22] calculated the next to leading order corrections to $\gamma\pi^- \to \pi^-\pi^0$ and $\eta \to \pi^+\pi^-\gamma$ in chiral perturbation theory. The corrections include one loop diagrams involving one vertex from the Wess-Zumino term, and tree diagrams from the $O(p^6)$ effective Lagrangian. The tree coefficients were fixed by assuming their saturation by vector meson contributions. The correction term has the following form

$$F^{3\pi}(s,t',u) = F^{3\pi}(0)\left(1 + C^{\pi^0}_{loops}(s,t',u) + \frac{1}{2m_\rho^2}(s+t'+u)\right)$$

where $C^{\pi^0}_{loops}(s,t',u)$ is the loop correction. For the $\gamma\pi^- \to \pi^-\pi^0$ reaction the loop contribution is similar in magnitude to higher dimension terms in the Lagrangian.

Figure 2 shows $F^{3\pi}(s,t',u)$ as a function of s for the models of Terent'ev[20] (solid curve), Rudaz[21] (short dashed curve), and Bijnens *et al.*[22] (long dashed curve) for $t' = u = 0$, and $\delta = 0$. Also shown are the amplitudes at zero momentum for N_c=4, 3, and 2, and the zero momentum VMD model of Cohen[11]. The calculations indicate that $F^{3\pi}$ grows with increasing s. The two VMD calculations show a larger increase than the χPT calculation. For the proposed measurement we expect corrections to the zero momentum amplitude to be in the 20% range.

B Background reactions

The experimental signature for the t-channel pion exchange mechanism of figure 1 will be the enhancement of the cross section at low t and $sin^2\theta_\pi$ angular distribution of the pion. The low t enhancement will be on top of relatively flat backgrounds produced by ρ^+ and $\pi\Delta$ final states. Given the relatively high statistics obtained in this measurement, it will be possible to reliably extract $\sigma_{\gamma\pi\to\pi\pi}$ cross sections even under worst-case situations where the signal-to-background is only 1:2. Background suppression should work especially well at high photon energies, approximately 2 GeV. In this section we present model calculations for the magnitude, and the s, t and θ_π distributions for these backgrounds.

There is little information available on $\gamma p \to \pi^+\pi^0 n$ background reactions. It is known that the $\gamma p \to \pi^+\pi^- p$ reaction is dominated by ρ^0 and $\Delta^{++}\pi^-$ final states over the photon energy range from approximately 1 to 2 GeV. Likewise for the $\gamma p \to \pi^+\pi^0 n$ reaction, we assume the dominance of ρ^+ and $\Delta\pi$ final states. Cross sections for $\gamma p \to \Delta^0\pi^+$ have been measured[23], and at $E_\gamma = 2.0$ GeV the cross section is approximately 2.5 μb. The reaction $\gamma p \to \Delta^+\pi^0$ has not been measured, and we assume its cross section is also equal to 2.5 μb. Barber*et al.*[24] have determined $\gamma p \to \rho^+ n$ cross sections in the energy range 2.4 to 4.8 GeV. Extrapolating their cross section curves to 2.0 GeV gives 5 μb. Summing the cross sections with the appropriate branching ratios gives a total estimated cross section of 7.5 μb at 2.0 GeV. This estimate is in good agreement with the $\gamma n \to \pi^-\pi^0 p$ data shown in Figure 13a[25].

To make estimates of the anticipated backgrounds, we modeled cross sections in the $\Delta\pi$ channel assuming isotropic distributions in the $\gamma p \to \Delta\pi$ and $\Delta \to \pi n$ center of mass frames. The total cross section for the $\Delta\pi$ channel we take as 5 μb equally weighted between $\Delta^0\pi^+$ and $\Delta^+\pi^0$ final states. This cross section is the average of our estimate and the amount of non-ρ^- cross section in the $\gamma n \to \pi^-\pi^0 p$ reaction[25]. To restrict background events we require that in the $\pi\pi$ center-of-mass frame $|cos\theta_\pi| < 0.6$. Furthermore, we require that the $\pi^+ n$ and $\pi^0 n$ invariant masses, M_{1n} and M_{2n}, should both be greater than 1.5 GeV. Since the background model assumes a $\Delta\pi$ intermediate state, this eliminates most events except for those on the high energy (> 1.5 GeV) tail of the Δ. For our analysis the Δ was modeled as a Breit-Wigner line shape. The cut inefficiency for true events varies from

0.38 at $s = 6m_\pi^2$ to 0.63 at $s = 16m_\pi^2$.

The other background reaction to consider is $\gamma p \rightarrow \rho^+ n$. Since diffractive production is not allowed in this case (the photon cannot spontaneously change into a ρ^+) other production mechanisms are responsible for ρ^+ production. Figures 13b and 13c show differential and total cross sections for $\gamma n \rightarrow \rho^- p$, respectively. The solid curves in the figures are meson exchange calculations for $\gamma n \rightarrow \rho^- p$. The figures show that the meson exchange mechanism alone cannot explain the data. At low $|t|$ the experimental differential cross sections are twice the size of the calculation. The agreement with the experimental total cross section is adequate only for photon energies above 2.5 GeV. Figure 13b also shows that the total ρ^- photo-production cross section peaks at approximately 1.5 GeV, or $W \approx 1.9$ GeV. This has led to speculation that much of the ρ^- production results from the decay of nucleon resonances[26].

For the background calculation we assume isotropic distributions in the $\gamma p \rightarrow \rho^+ n$ and $\rho^+ \rightarrow \pi^+ \pi^0$ center of mass frames. This is consistent with a ρ^+ production mechanism through N^* decay. The total cross section at 2.0 GeV was taken as 5 μb. The same cuts as discussed above were applied to the cross sections. Figure 14 is a plot of the $\sqrt{s}$ distribution of the $\pi^- \pi^0$ data. The fitted curves, which show the ρ^- peak and $\Delta\pi$ backgrounds, give little evidence for ρ^- strength in the threshold region ($\sqrt{s} \approx 500$ MeV). In the analysis of Benz *et al.* the ρ^- peak was fitted with a line shape that in the threshold region has the approximate form $(s - 4m_\pi^2)\Gamma_{BW}(s)$, where $\Gamma_{BW}(s)$ is the Breit-Wigner form. We used this form of the ρ^+ peak for our analysis.

Figure 15 is a plot of $d^2\sigma/dtds$ as a function of s at $E_\gamma = 2.0$ GeV and $t = -m_\pi^2$, where the cross sections have been reduced by cut inefficienies, and and we have assumed the model of Terent'ev for the momentum dependence of $F^{3\pi}$. The dashed curve in the figure with error bars are the calculated cross sections for $\gamma p \rightarrow \Delta\pi \rightarrow \pi^+ \pi^0 n$ reduced by the cuts. The calculated cross sections for $\gamma p \rightarrow \rho^+ n$ are shown as the long-dashed curve in the figure. Based on our model assumptions, the figure indicates that acceptable signal-to-background ratios can be obtained for values of s down to 10 m_π^2.

To summarize the discussion in this appendix, we have presented evidence that background reactions can be minimized and that signal-to-background ratios of 1:1 or better can be obtained. The calculations presented here are purely phase space, and we implicitly assume the matrix element <

$\gamma p|T_{fi}|\pi^+\pi^0 n >$ is constant. This does not include the effects of nucleon structure and reaction mechanisms that will modulate uniform phase space distributions. By using real data to carefully examine background reactions, it will be possible to improve upon the conditions estimated here for the extraction of the t-channel π-exchange cross section.

References

[1] S. Weinberg, Physica **96A**, 327 (1979).

[2] "Dynamics of the Standard Model", J. F. Donoghue, E. Golowich, B. R. Holstein, Cambridge (1992).

[3] J. Gasser, and H. Leutwyler, Ann. Phys. **150**, 142 (1984); Nucl. Phys. **B250**, 465 (1985).

[4] B. R. Holstein, Nucl. Phys. A **546**, 213c (1992), and references therein.

[5] S. L. Adler, Phys. Rev. **177**, 2426 (1969); J. S. Bell and R. Jackiw, Nuovo Cimento **60A**, 47 (1969).

[6] J. Wess and B. Zumino, Phys. Lett. **37B**, 95 (1971).

[7] E. Witten, Nucl. Phys. **B223**, 422 (1983).

[8] S. L. Adler, B. W. Lee, S. B. Treiman, and A. Zee, Phys. Rev. **D4**, 3497 (1971).

[9] M. Terent'ev, JETP Lett. **14**, 94 (1971).

[10] R. Aviv and A. Zee, Phys. Rev. **D5**, 2372 (1972).

[11] T. D. Cohen, Phys. Lett. **233**, 467 (1989).

[12] Yu. M. Antipov *et al.*, Phys. Rev. D **36**, 21 (1987).

[13] Ya. Pomeranchuk and I. M. Shmushkevich, Nucl. Phys. **23**, 452 (1961).

[14] G. S. Iroshnikov and Yu. P. Nikitin, Sov. J. Nucl. **7**, 381 (1968).

[15] T. A. Aibergenov *et al.*, Proceedings of the Lebedev Physics Institute, Academy of Sciences of the U.S.S.R., **186**, 169 (1988).

[16] Experiments E89-004 (R. Schumacher spokesman), E89-024 (G. Mutchler spokesman), E91-008 (B. Ritchie spokesman), and E93-033 (J. Napolitano spokesman).

[17] CEBAF Conceptual Design Report, 1990.

[18] G. F. Chew, and F. E. Low, Phys. Rev. **113**, 1640 (1959).

[19] Private communication, J. Napolitano.

[20] M. V. Terent'ev, Phys. Lett. **38B**, 419 (1972).

[21] S. Rudaz, Phys. Rev. D **10** 3857 (1974).

[22] J. Bijnens, A. Bramon, and F. Cornet, Phys. Lett. **237B**, 488 (1990).

[23] Crouch *et al.*, PR **163**, 1510 (1967); Erbe *et al.*, PR **175**, 1669 (1968); Struczinski *et al.*, Nucl. Phys. **B108**, 45 (1976).

[24] D. P. Barber, *et al.*, Z. Physik C **2**, 1 (1979).

[25] P. Benz, *et al.*, Nucl. Phys. **B79**, 10 (1974).

[26] Letter of intent to CEBAF PAC8, Spokespersons J. P. Connelly, and P. L. Cole.

[27] Proposal to CEBAF PAC8, Spokesperson B. Norum.

Table 1: Acceptance in percent as a function of s and t at $E_\gamma = 1.5GeV$ and $B = 0.2B_0$. The acceptance calculation was based on 1000 input events per kinematic point.

		$s(m_\pi^2)$				
		6	8	10	12	14
$t(m_\pi^2)$	-1	7	16	19	21	25
	-3	14	15	21	22	25
	-5	16	20	21	26	24
	-7	24	21	25	24	25
	-9	27	24	24	23	28

Table 2: Acceptance in percent as a function of s and E_γ at $t = -m_\pi^2$ and $B = 0.2B_0$. The acceptance calculation was based on 1000 input events per kinematic point.

		$s(m_\pi^2)$				
		6	8	10	12	14
$E_\gamma(GeV)$	1.00	20	22	27	23	26
	1.25	15	18	26	24	27
	1.50	13	13	20	23	21
	1.75	7	11	15	19	22
	2.00	3	7	12	15	17

List of Figures

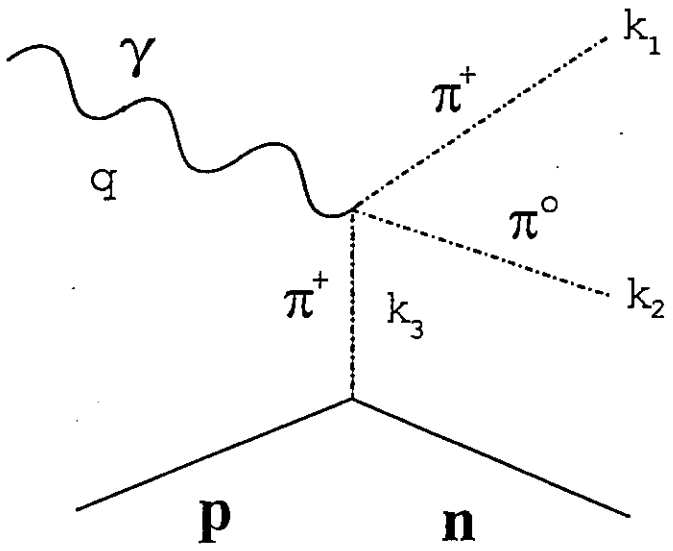

Figure 1: t-channel Feynman diagram for $\gamma\pi^+ \to \pi^+\pi^0$.

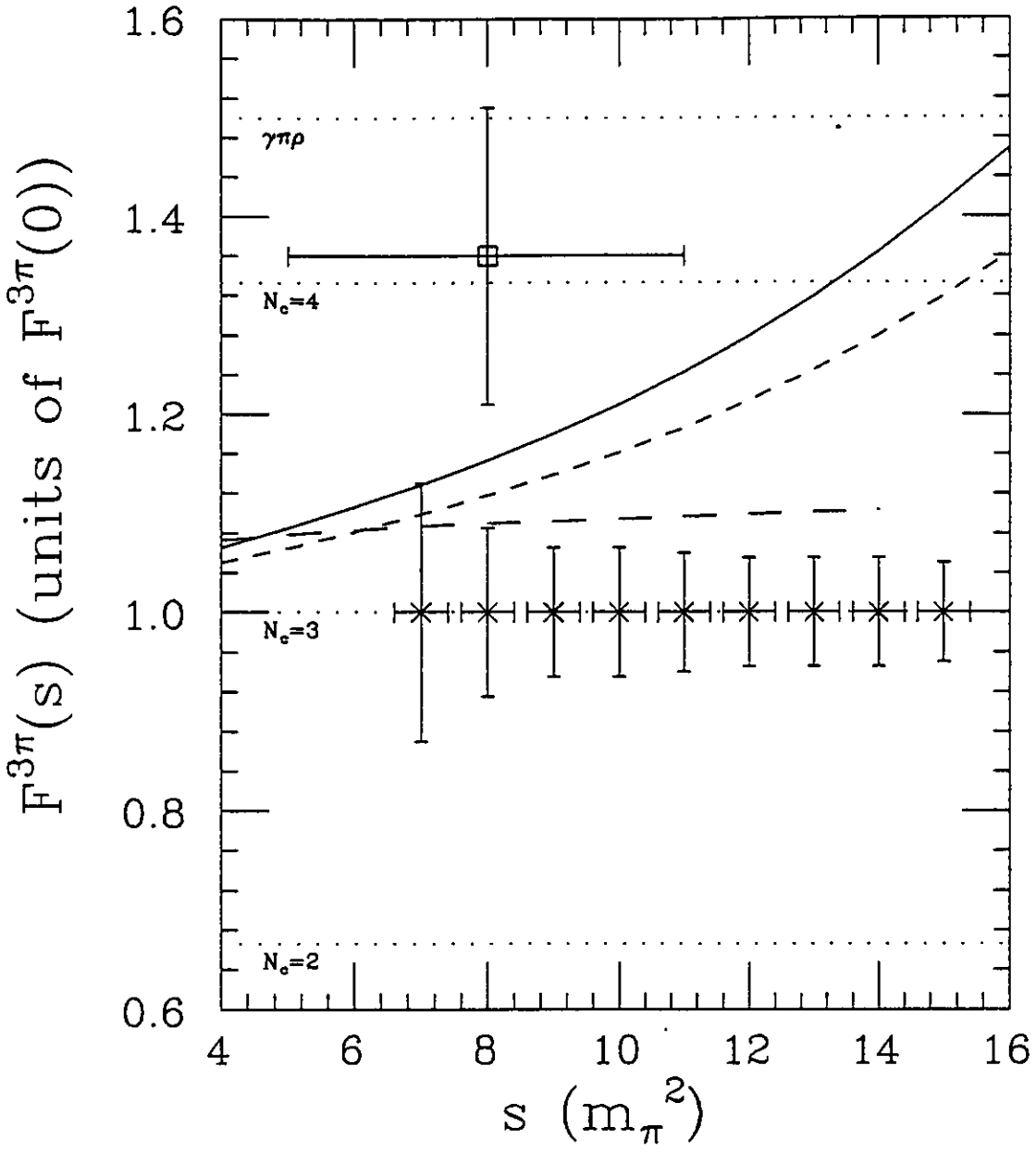

Figure 2: The $\gamma \to 3\pi$ structure function $F^{3\pi}(s,t',u)$ as a function of s for the models of Terent'ev[21] (solid curve), Rudaz[22] (short-dashed curve), and for Bijnens *et al.*[23] (long-dashed curve), for $t' = u = 0$ and $\delta = 0$. The dotted lines show the amplitudes for $N_c = 4$, $N_c = 3$, and $N_c = 2$. Also shown is the low energy limit of a $\gamma \to \pi\rho \to 3\pi$ calculation[12]. The square data point is from Antipov *et al.*[16] The other data points show the anticipated statistical and systematic uncertainties for the proposed measurement.

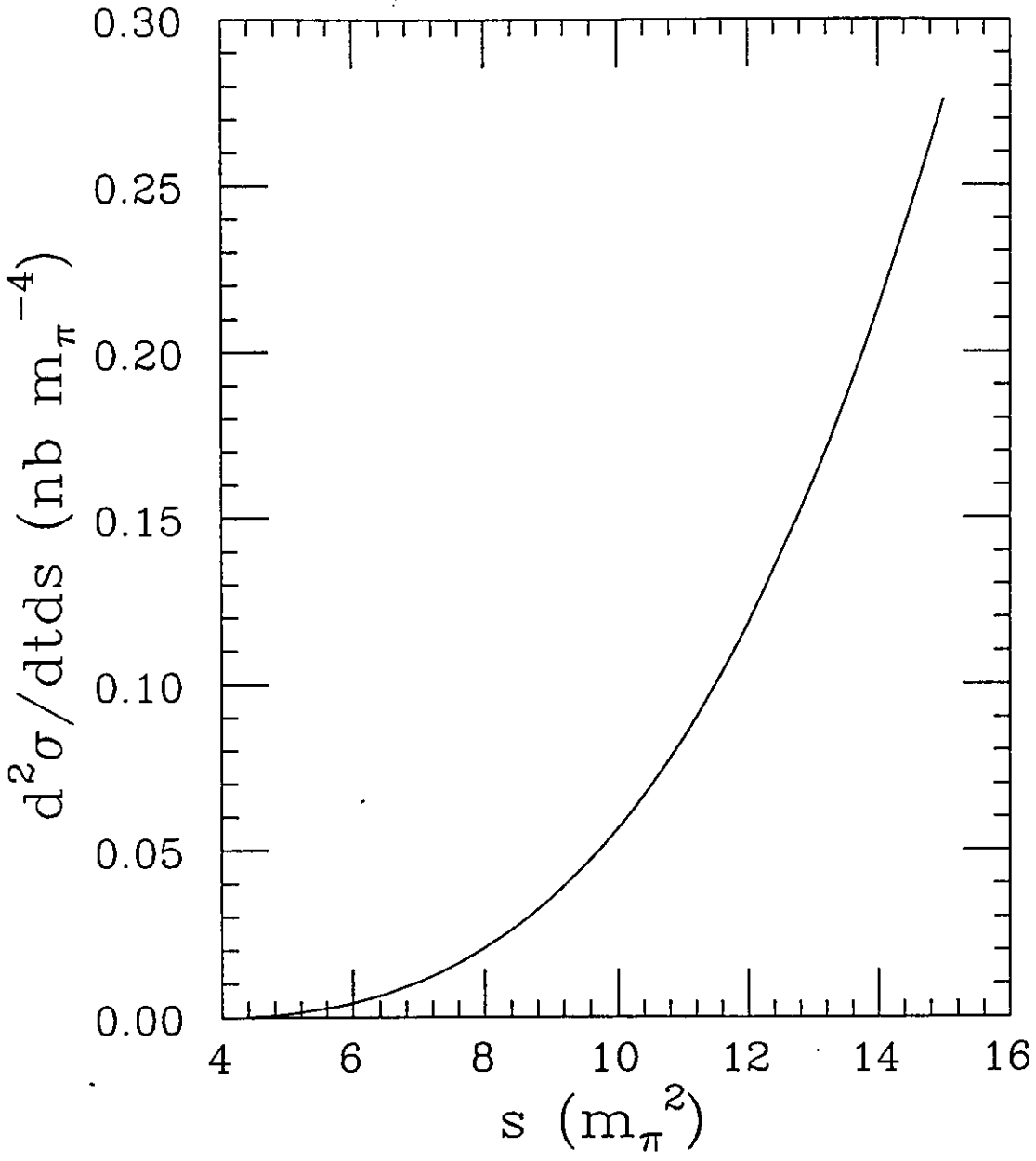

Figure 3: $d^2\sigma/dtds$ as a function of s for $E_\gamma = 1.5\ GeV$, $t = -m_\pi^2$, and $F^{3\pi} = 9.5\ GeV^3$.

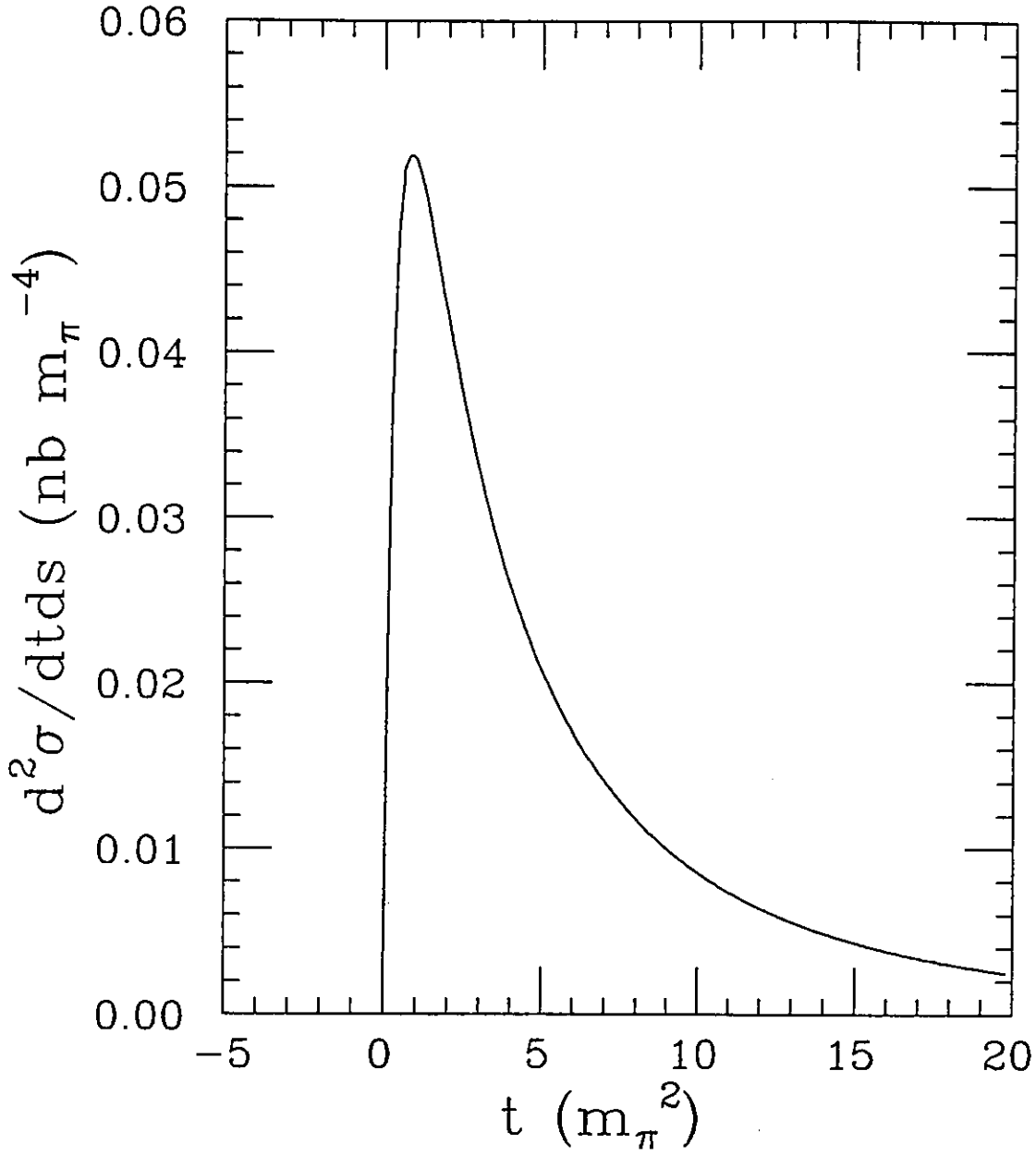

Figure 4: $d^2\sigma/dtds$ as a function of t for $E_\gamma = 1.5\ GeV$, $s = 10m_\pi^2$, and $F^{3\pi} = 9.5\ GeV^3$.

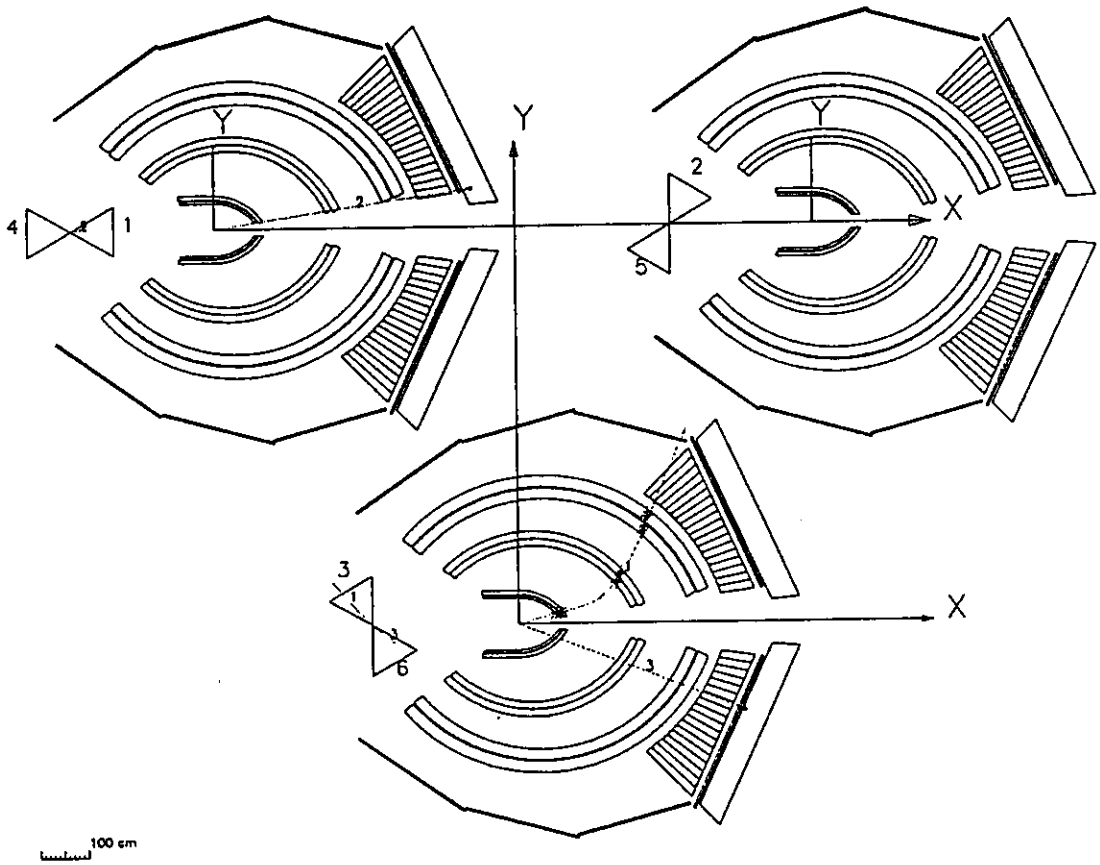

Figure 5: One event display for $\gamma p \to \pi^+\pi^0 n$ event.

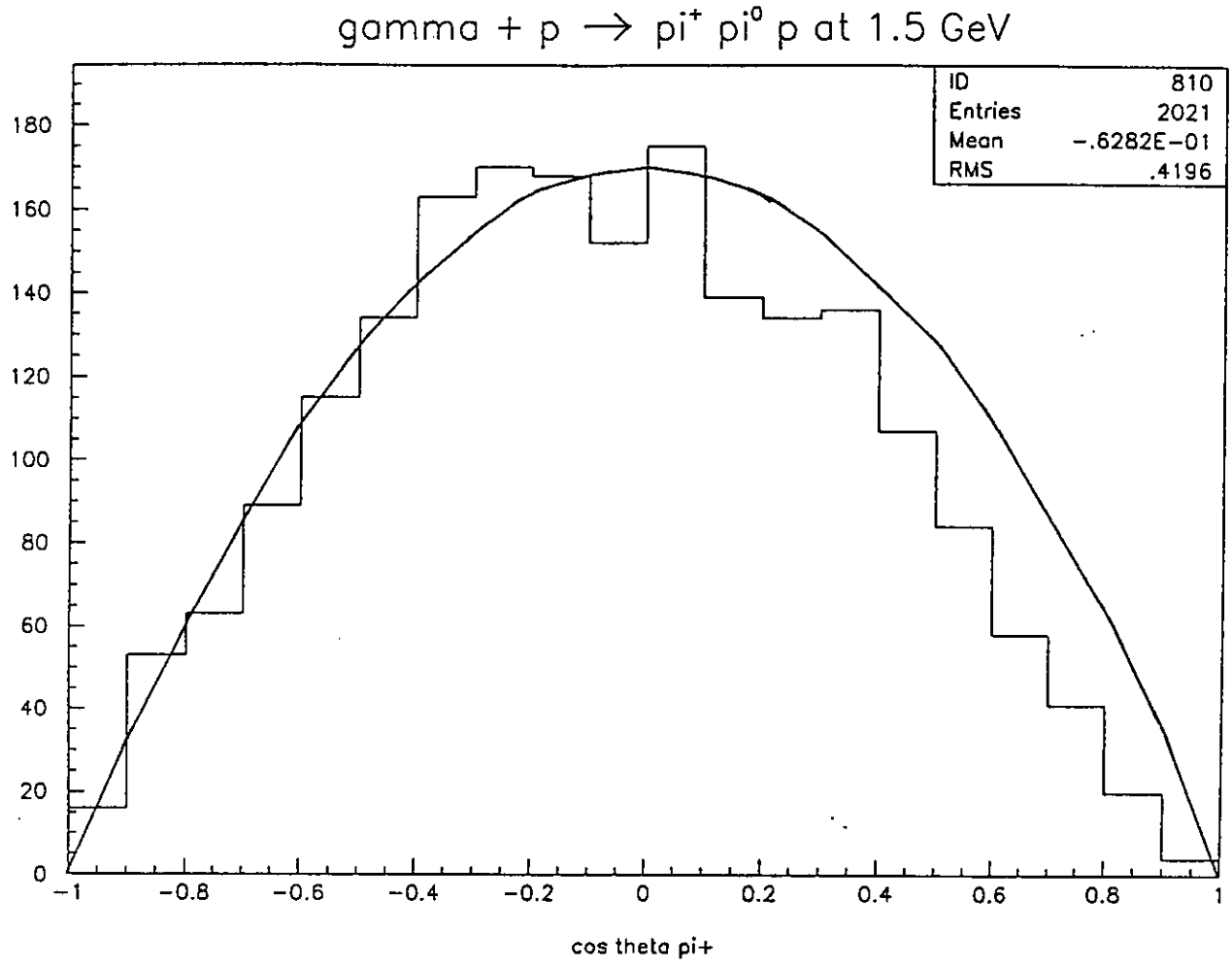

Figure 6: The π^+ angular distribution for accepted events in the $\pi^+\pi^0$ center-of-mass frame for $s = 10\ m_\pi^2$ and t distributed as given by Equation 1. The solid curve in the figure shows $sin^2\theta$ with arbitrary normalization.

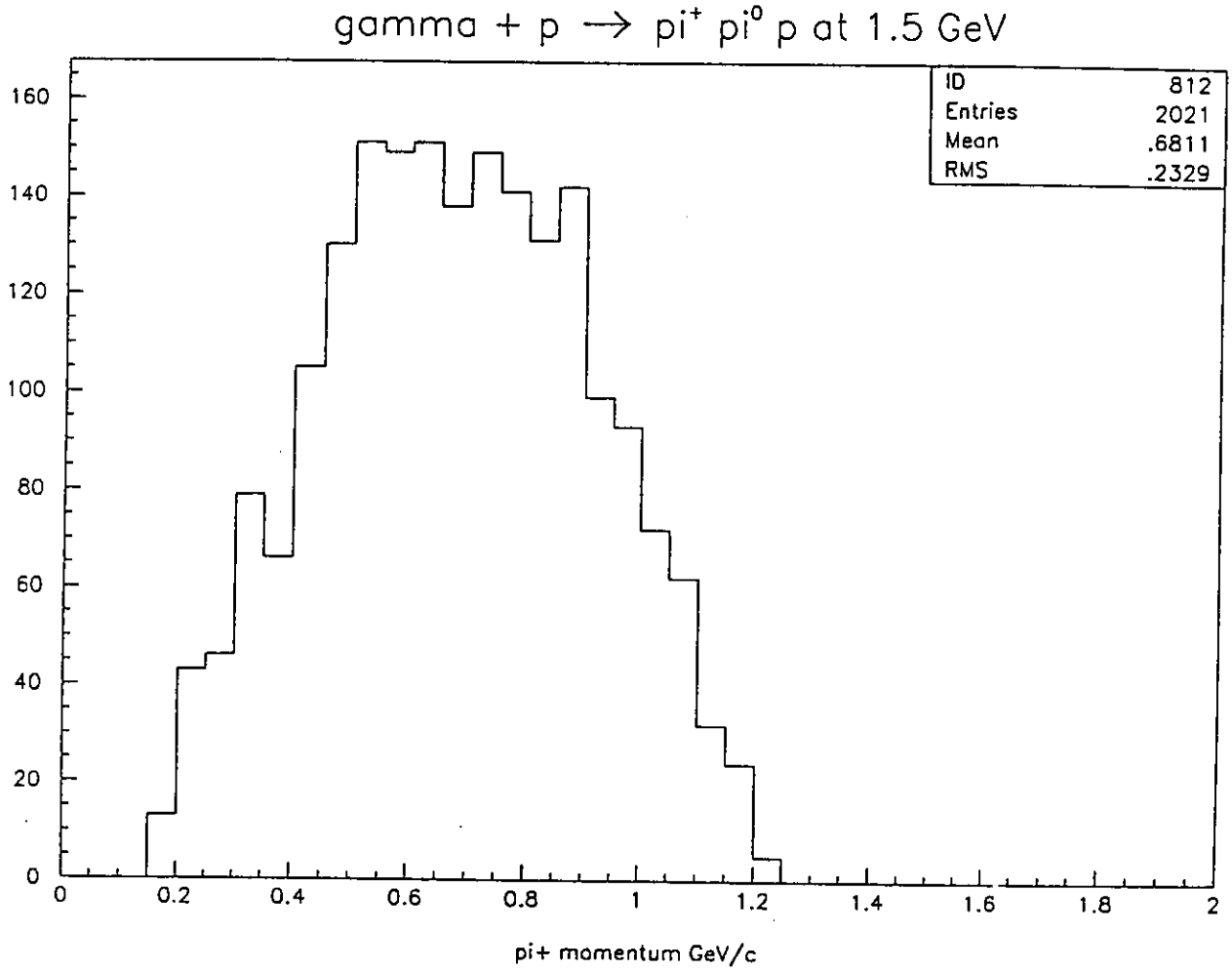

Figure 7: π^+ momentum distribution for accepted events at $E_\gamma = 1.5$ GeV.

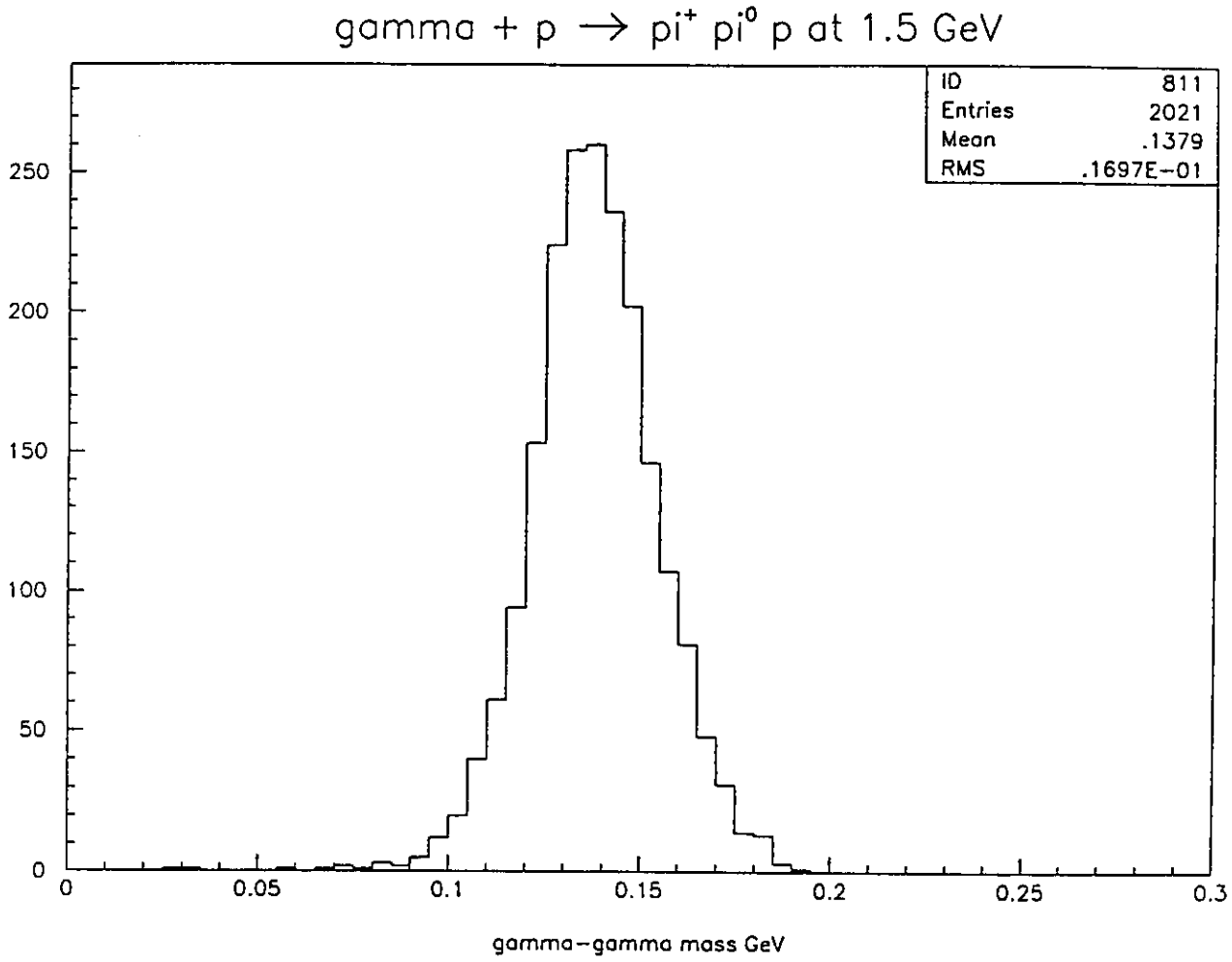

Figure 8: Two-photon invariant mass distribution from $\pi^0 \rightarrow \gamma\gamma$

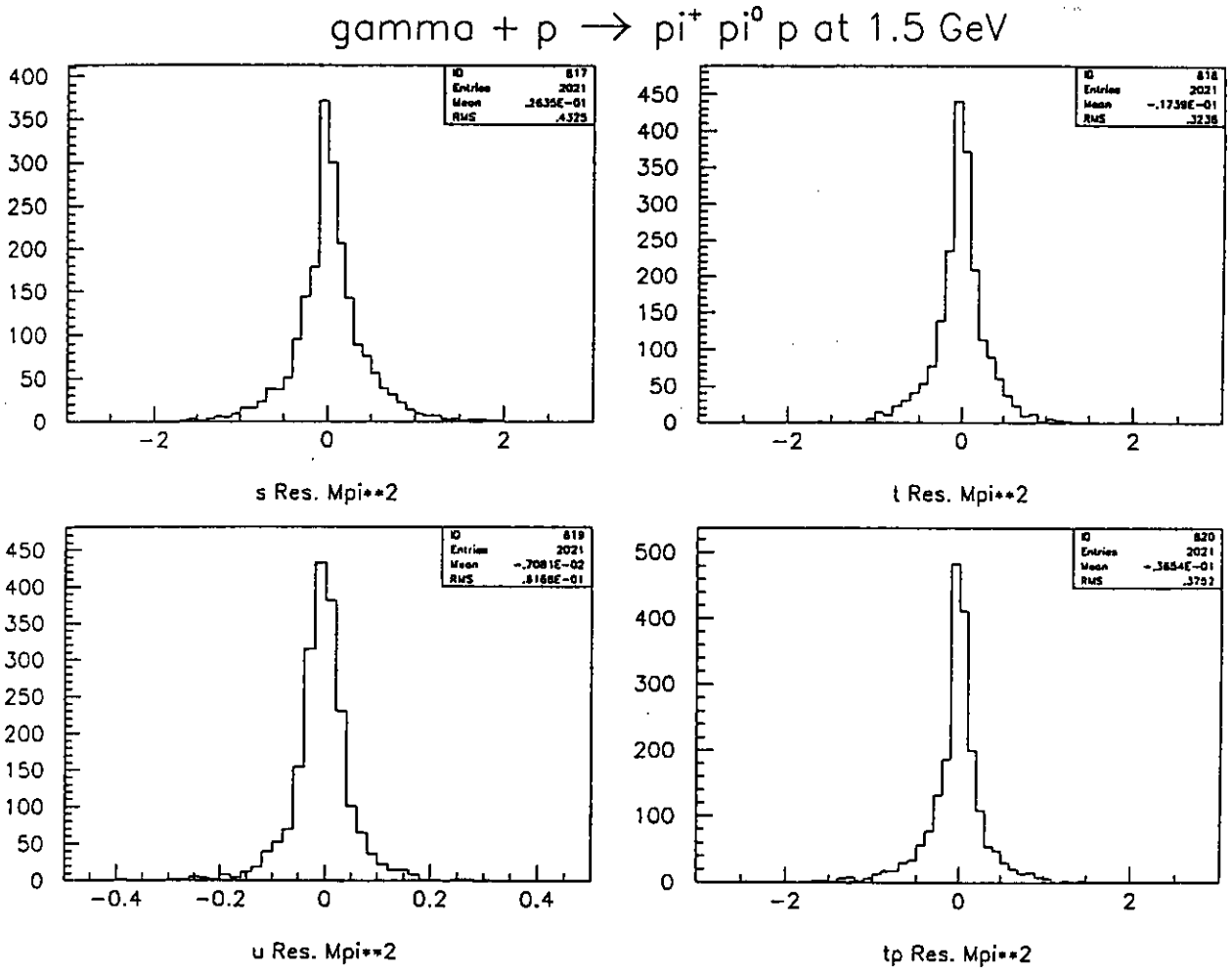

Figure 9: Resolution functions for t, s, t', and u at $s = 10m_\pi^2$, and $E_\gamma = 1.5$ GeV.

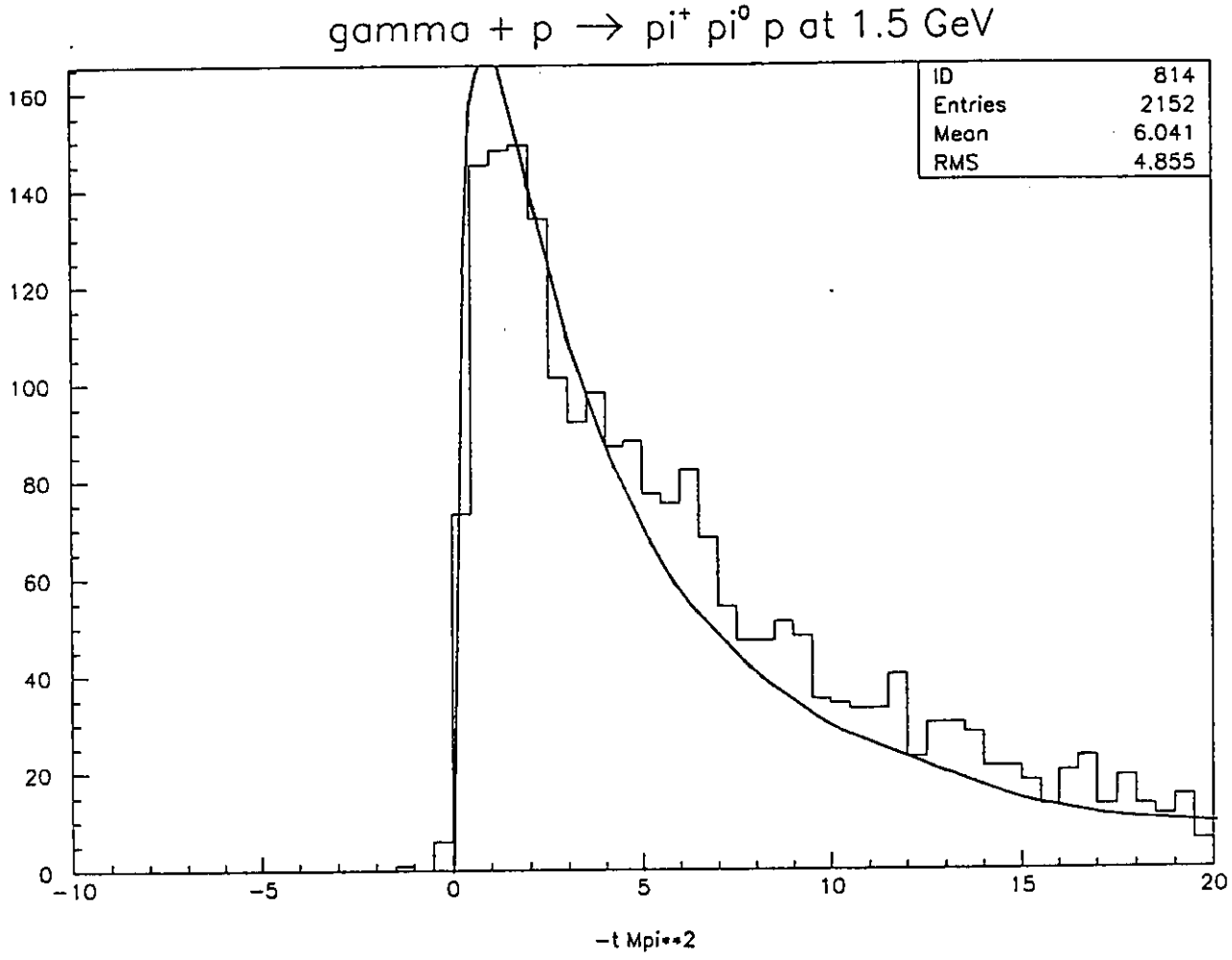

Figure 10: t distribution of accepted events at $s = 10\ m_\pi^2$ and $E_\gamma = 1.5$ GeV. The solid curve is the t dependence of Equation 1 scaled to the data at $t = -2m_\pi^2$.

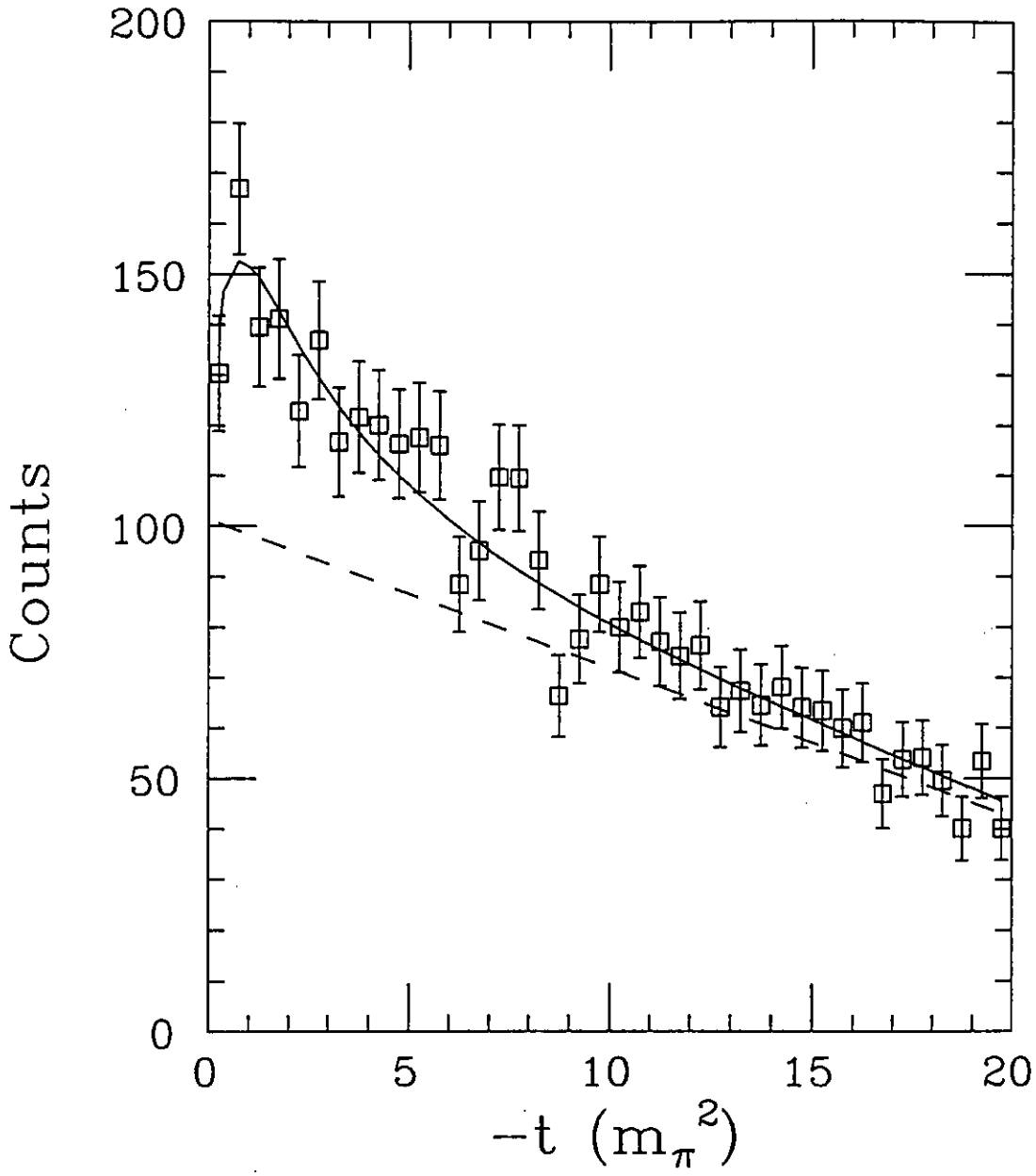

Figure 11: Simulated data and backgrounds assuming 100 signal events/m_π^2 at $t = -m_\pi^2$ and a worst-case signal-to-background ratio of 1:2. The solid curve shows the fit to the total, and the dashed curve shows the fitted background.

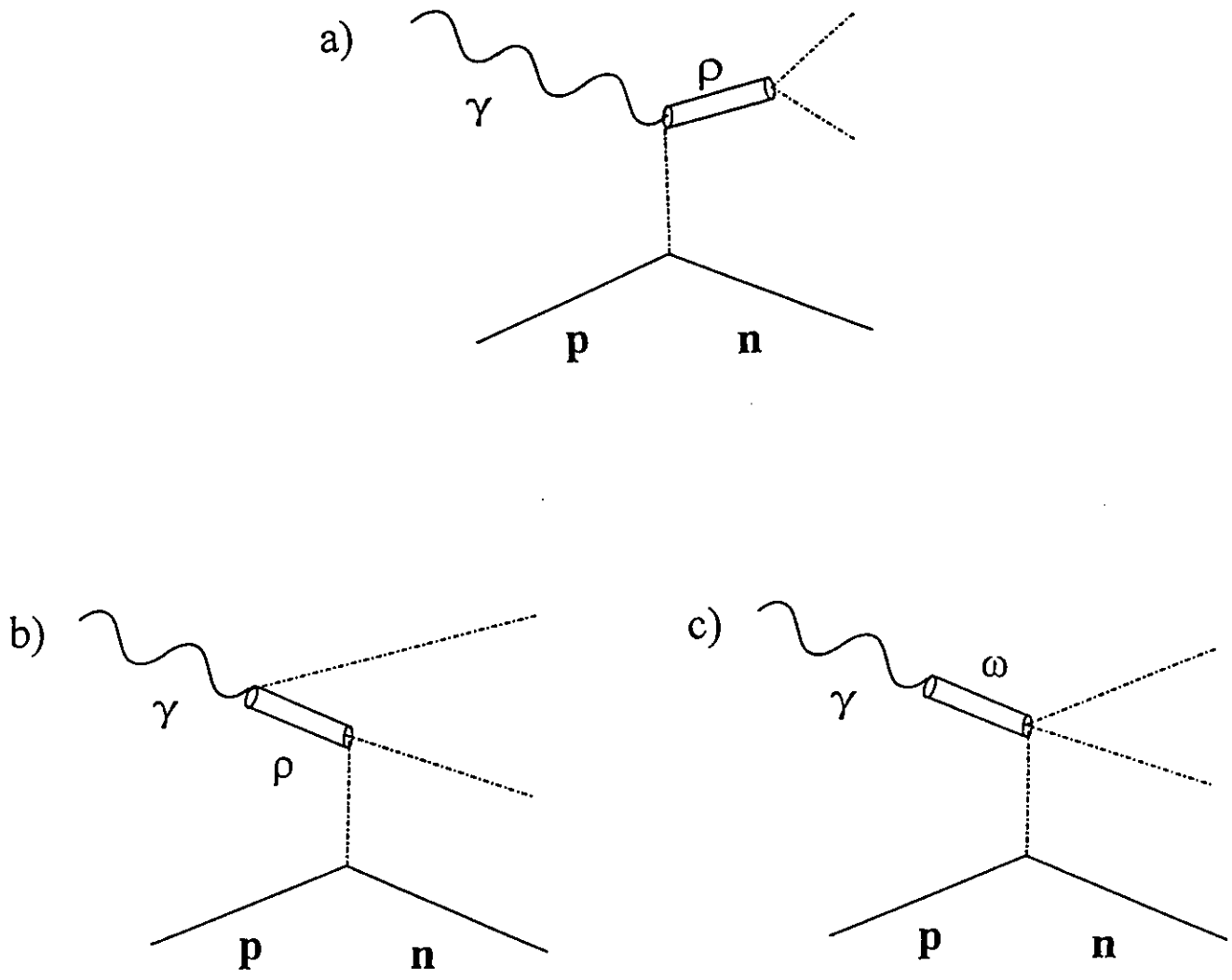

Figure 12: Vector meson pole diagrams for $\gamma\pi^+ \to \pi^+\pi^0$.

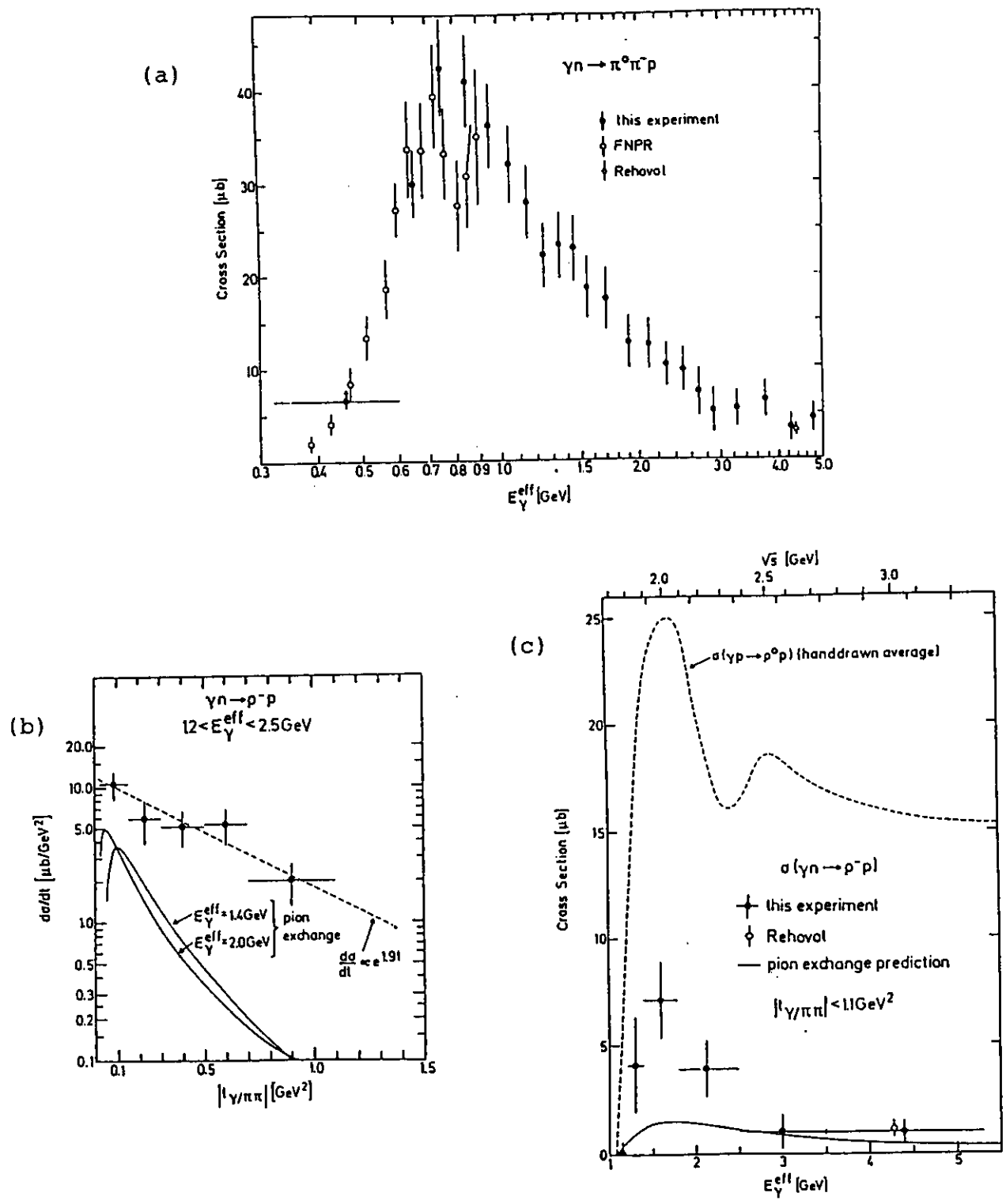

Figure 13: $\gamma n \to \pi^+\pi^0 p$ cross sections from Benz *et al.*[26] (a) Total cross sections for $\gamma n \to \pi^+\pi^0 p$. (b) Differential cross sections for $\gamma n \to \rho^- p$. (c) Total cross sections for $\gamma n \to \rho^- p$.

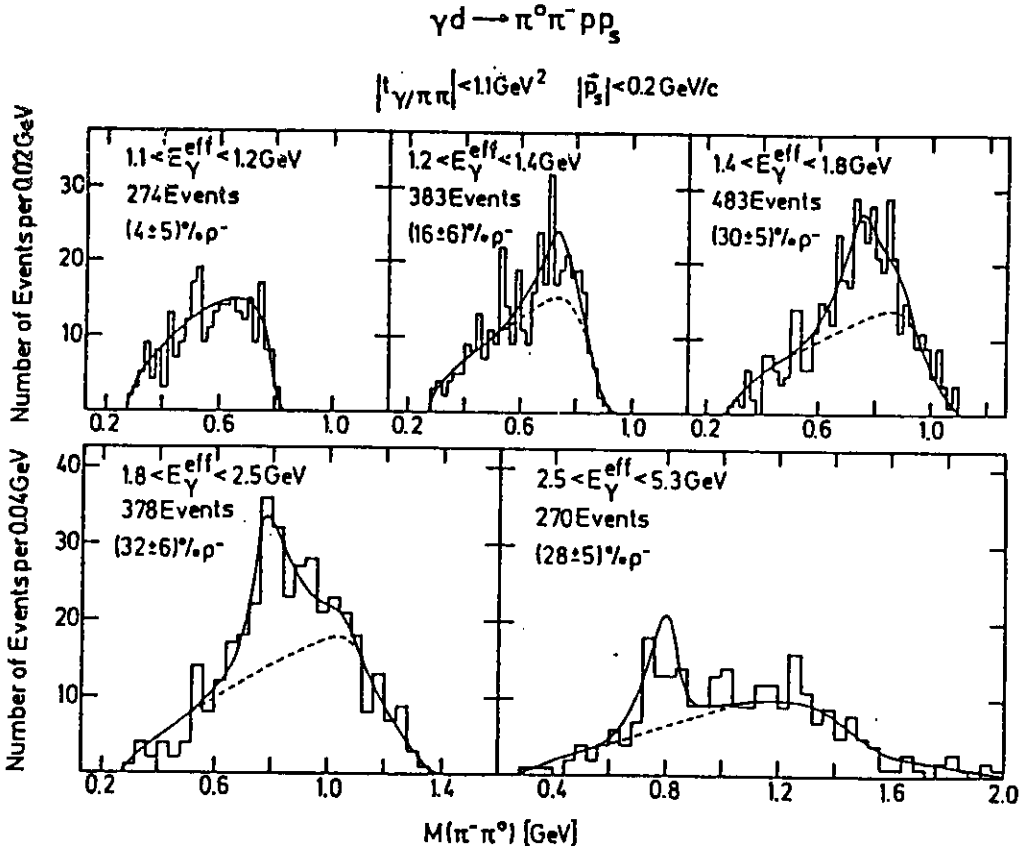

Figure 14: The mass distribution for $\pi^-\pi^0$ events is shown for different photon energy ranges[26]. The curves show fits assuming ρ^- and $\Delta\pi$ backgrounds.

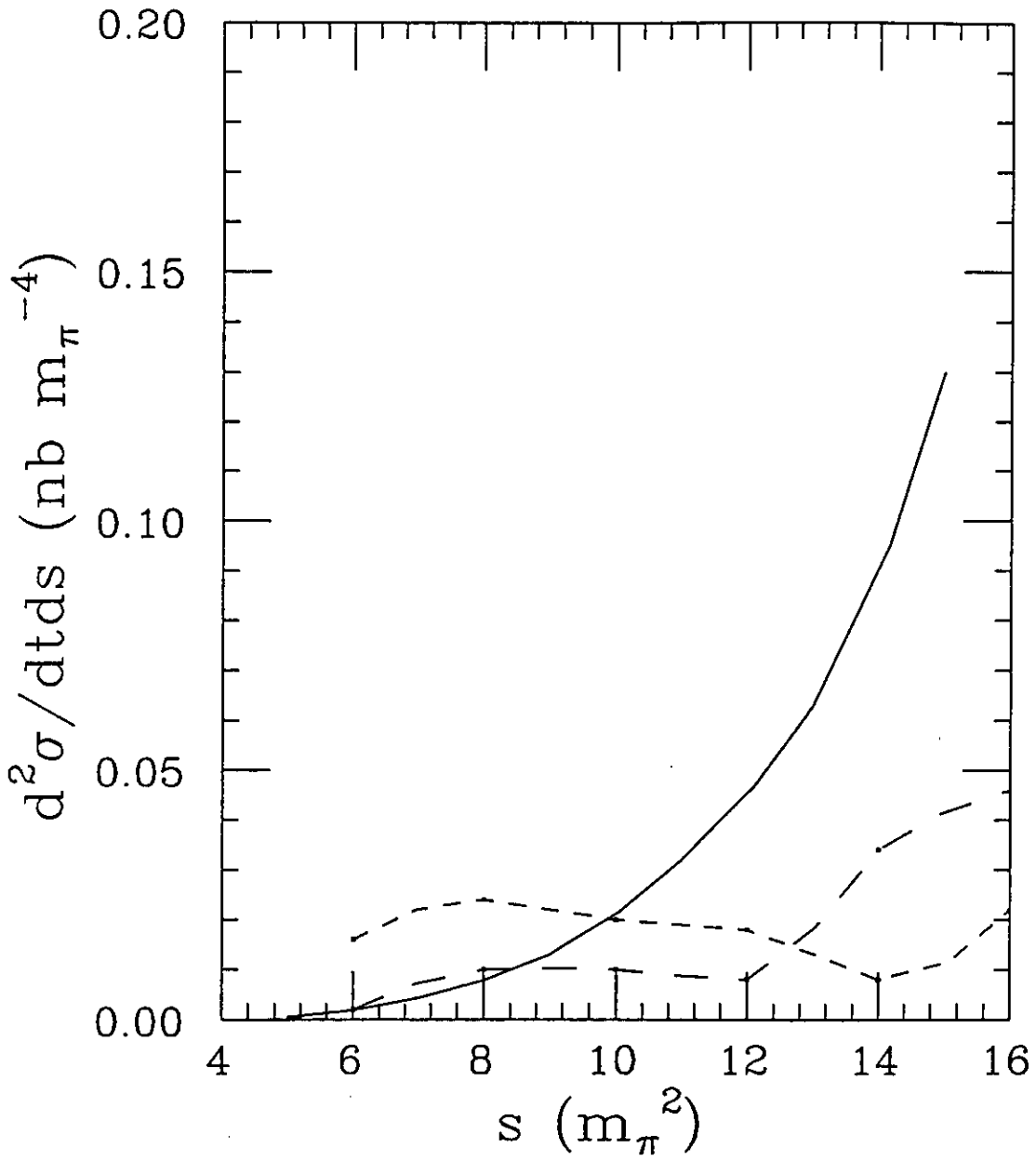

Figure 15: Signal and background cross sections reduced by cut inefficiencies versus s for $E_\gamma = 2.0$ GeV and $t = -m_\pi^2$. The solid curve is the cross section from Equation 1 using $F^{3\pi}$ from Terent'ev[21]. The short-dashed curve with errors is the cross section for $\gamma p \to \Delta\pi$. The long-dashed curve is the cross section for $\gamma p \to \rho^+ n$.

HAZARD IDENTIFICATION CHECKLIST

CEBAF Experiment: PR-94-015 Date: 6/6/94

Check all items for which there is an anticipated need—do not check items that are part of the CEBAF standard experiment (HRSE, HRSH, CLAS, HMS, SOS in standard configurations).

Cryogenics
- _____ beamline magnets
- _____ analysis magnets
- _____ target
- _____ drift chambers
- _____ other

Electrical Equipment
- _____ cryo/electrical devices
- _____ capacitor banks
- _____ high voltage
- _____ exposed equipment

Radioactive/Hazardous Materials
List any radioactive or hazadorous/ toxic materials planned for use:
_____
_____

Pressure Vessels
- _____ inside diameter
- _____ operating pressure
- _____ window material
- _____ window thickness

Flammable Gas or Liquids
(incl. target)
type: Liquid hydrogen
flow rate: _____
capacity: _____
Saclay target

Other Target Materials
- ___ Beryllium (Be)
- ___ Lithium (Li)
- ___ Mercury (Hg)
- ___ Lead (Pb)
- ___ Tungsten (W)
- ___ Uranium (U)
- ___ Other (list below)

_____
_____

Vacuum Vessels
- _____ inside diameter
- _____ operating pressure
- _____ window material
- _____ window thickness

Radioactive Sources
- _____ permanent installation
- _____ temporary use

type: _____
strength: _____

Large Mech. Structure/System
- _____ lifting devices
- _____ motion controllers
- _____ scaffolding or elevated platforms
- _____ other

Lasers
type: _____
wattage: _____
class: _____

Installation
- _____ permanent
- _____ temporary

Use
- _____ calibration
- _____ alignment

Hazardous Materials
- ____ cyanide plating materials
- ____ scintillation oil (from)
- ____ PCBs
- ____ methane
- ____ TMAE
- ____ TEA
- ____ photographic developers
- ____ other (list below)

_____
_____
_____

Notes:
_____
_____
_____
_____
_____
_____